European Journal of Pharmaceutical Sciences 175 (2022) 106216

Contents lists available at ScienceDirect

European Journal of Pharmaceutical Sciences

journal homepage: www.elsevier.com/locate/ejps

Characterization of phospholipid-modified lung surfactant *in vitro* and in a neonatal ARDS model reveals anti-inflammatory potential and surfactant lipidome signatures

Sarah Kupsch [a,1], Lars F. Eggers [b,1], Dietmar Spengler [c], Nicolas Gisch [b], Torsten Goldmann [d,e], Heinz Fehrenbach [f,e], Guido Stichtenoth [g], Martin F. Krause [c], Dominik Schwudke [b,e,h,i], Andra B. Schromm [a,i,*]

[a] Division of Immunobiophysics, Priority Area Infections, Research Center Borstel, Leibniz Lung Center, Borstel, Germany
[b] Division of Bioanalytical Chemistry, Priority Area Infections, Research Center Borstel, Leibniz Lung Center, Borstel, Germany
[c] Department of Pediatrics, University Hospital of Schleswig-Holstein, Kiel, Germany
[d] Campus Luebeck and the Research Center Borstel, Pathology of the University Medical Center Schleswig-Holstein (UKSH), Borstel, Germany
[e] Airway Research Center North (ARCN), Member of the German Center for Lung Research (DZL), Großhansdorf, Germany
[f] Division of Experimental Pneumology, Priority Area Asthma and Allergies, Research Center Borstel, Leibniz Lung Center, Borstel, Germany
[g] Department of Pediatrics, University Hospital of Schleswig-Holstein, Luebeck, Germany
[h] German Center for Infection Research (DZIF), Thematic Translational Unit Tuberculosis, Partner Site Hamburg-Lübeck-Borstel-Riems, Germany
[i] Kiel Nano, Surface and Interface Science KiNSIS, Kiel University, Germany

ARTICLE INFO

Keywords:
Pulmonary surfactant
Lipidomics
Anionic phospholipids
Lipopolysaccharide
Macrophages
Inflammasome

ABSTRACT

A strong inflammatory immune response drives the lung pathology in neonatal acute respiratory distress syndrome (nARDS). Anti-inflammatory therapy is therefore a promising strategy for improved treatment of nARDS. We demonstrate a new function of the anionic phospholipids POPG, DOPG, and PIP2 as inhibitors of IL-1β release by LPS and ATP-induced inflammasome activation in human monocyte-derived and lung macrophages. Curosurf® surfactant was enriched with POPG, DOPG, PIP2 and the head-group derivative IP3, biophysically characterized and applicability was evaluated in a piglet model of nARDS. The composition of pulmonary surfactant from piglets was determined by shotgun lipidomics screens. After 72 h of nARDS, levels of POPG, DOPG, and PIP2 were enhanced in the respective treatment groups. Otherwise, we did not observe changes of individual lipid species in any of the groups. Surfactant proteins were not affected, with the exception of the IP3 treated group. Our data show that POPG, DOPG, and PIP2 are potent inhibitors of inflammasome activation; their enrichment in a surfactant preparation did not induce any negative effects on lipid profile and reduced biophysical function *in vitro* was mainly observed for PIP2. These results encourage to rethink the current strategies of improving surfactant preparations by inclusion of anionic lipids as potent anti-inflammatory immune regulators.

1. Introduction

Neonatal acute respiratory distress syndrome (nARDS)[2] is a life-threatening condition in newborns caused by insufficient lung mechanics and oxygenation, acute inflammation, tissue destruction and fibrotic tissue remodeling. nARDS has been acknowledged by clinicians

* Corresponding author at: Division of Immunobiophysics, Priority Area Infections, Research Center Borstel, Leibniz Lung Center, Borstel, Germany.
E-mail address: aschromm@fz-borstel.de (A.B. Schromm).

[1] These authors contributed equally to this work.

[2] **Abbreviations:** AD, *A. dest*, ALI, acute lung injury; BAL, bronchoalveolar lavage; DAG, diacylglycerol; DOPC, 18:1-(Δ9-*cis*)-phosphatidylcholine; DOPG, 18:1-(Δ9-*cis*)-phosphatidylglycerol; DPPC, 16:0 phosphatidylcholine; EU, endotoxin unit; IL-1β, interleukin-1β; IP3, inositol-1,2,6-triphosphate; LPS, lipopolysaccharide; nARDS, neonatal acute respiratory distress syndrome; NFκB, nuclear factor kappa B; PC, phosphatidylcholine; PE, phosphatidylethanol-amine; PG, phosphatidylglycerol; PI, phosphatidylinositol; PIP2, dipalmitoyl-phosphatidylinositol 3,5-bisphosphate; POPC, 16:0/18:1- phosphatidylcholine; POPG, 16:0/18:1 phosphatidylglycerol; PS, phosphatidylserine; SAXS, small-angle X-ray diffraction; SM, sphingomyelin; SP, surfactant protein; TLR4, Toll-like receptor 4.

https://doi.org/10.1016/j.ejps.2022.106216
Received 21 December 2021; Received in revised form 27 April 2022; Accepted 20 May 2022
Available online 23 May 2022

as a specific disease entity for many years (Faix et al., 1989) and in 2017, "the Montreux definition of nARDS" was finally reported by an international expert panel (De Luca et al., 2017). Of note, nARDS is to be distinguished from the respiratory distress syndrome (RDS) of the premature infant suffering from primary surfactant deficiency in an early stage of lung development. In nARDS, Toll-like-Receptor (TLR) 4-dependent signaling (Preuss et al., 2012a), neutrophil recruitment, inflammasome activation (Kolliputi et al., 2012), apoptosis, and pyroptosis (Bem et al., 2010) are hallmarks of the hyper-inflammatory cellular response. Massive degradation of endogenous surfactant by pulmonary phospholipases (especially by secretory phospholipase A2) (De Luca et al., 2013) requires surfactant supplementation to maintain lung function. To date, surfactant therapy is the only approved clinical intervention for the treatment of nARDS (Amigoni et al., 2017).

Besides the well investigated biophysical function of pulmonary surfactant, increasing evidence is raised for additional immunological functions of surfactant lipids. Anionic phospholipid species have been shown to be efficient inhibitors of TLR4-dependent intracellular signaling and release of the pro-inflammatory mediators tumor-necrosis-factor α (TNFα) and nitric oxide (NO) (Kuronuma et al., 2009). Specifically, 16:0/18:1 phosphatidylglycerol (POPG) has been identified as a potent immune regulator of lipopolysaccharide (LPS)-dependent activation of TLR4, assigning this lipid species an important function in the immunological homeostasis of the lung. In contrast to the adult lung, in the lung of pre-term and healthy neonates and in patients with respiratory distress syndrome the abundance of phosphatidylglycerol (PG) species is extremely low (Hallman and Gluck, 1976), with low levels of POPG and hardly detectable amounts of 18:1/18:1 PG (DOPG). Interestingly, earlier studies showed that PG-deficiency does not negatively affect the biophysical properties of the surfactant film but PG is compensated by phosphatidylinositol (PI) (Beppu et al., 1983). Inhibitory potential on TLR4 activation was also suggested for PI (Akashi et al., 2000). Supplementation of these lipid species may therefore be of benefit especially in newborns and contribute to reduce inflammation and contain the accompanying pathophysiology of nARDS.

Inflammasome activation is suggested to play a crucial role in the complex pathologies of nARDS, acute lung injury (ALI), chronic obstructive pulmonary disease (COPD), and other pulmonary diseases (Borthwick, 2016; Dolinay et al., 2012; Grailer et al., 2014; Kolliputi et al., 2012). Interleukin-1β (IL-1β) is a central downstream mediator produced upon canonical activation of the NLRP3 inflammasome which can be activated in macrophages by various danger signals. In the context of Gram-negative infections, LPS in combination with adenosine triphosphate (ATP) triggers canonical inflammasome activation resulting in IL-1β release (He et al., 2016). Activation depends on a two-signal-sequence: TLR4-activation is required for the NF-kB dependent production of pro-IL-1β and caspase-1 (signal 1) and ATP-triggered K^+ efflux induces inflammasome complex formation resulting in processing and release of the active cytokine (signal 2). So far, immune regulatory functions of surfactant lipids on inflammasome activation are mainly unexplored.

Our hypothesis for this study was that anionic surfactant components can modulate inflammasome activation and may therefore be beneficial to control inflammation in lung disease. To investigate this hypothesis, we analyzed the effects of a set of defined PG and PI molecular species and known signaling molecules on cell activation. To address different activation pathways, we included PGs, which have been shown to modulate the TLR4-NFκB signaling axis (Kuronuma et al., 2009; Numata et al., 2012b) and dipalmitoyl-phosphatidylinositol 3, 5-bisphosphate (PIP2) and inositol-1,2,6-trisphosphate (IP3) as candidates to modulate the sphingomyelinase ceramide axis of inflammasome activation (Kolliputi et al., 2012). In a second step, a commercially available porcine surfactant preparation (poractant alfa, Curosurf®, Chiesi) was enriched with these compounds. To determine functionality and applicability of the modified surfactant, preparations were characterized for biophysical properties and an *in vivo* application study was performed using a well-established triple-hit model of nARDS in newborn piglets (Preuss et al., 2012b). The porcine immune system resembles the immune response in the human lung in many aspects and is therefore a highly suitable model (Mair et al., 2014).

2. Materials and methods

2.1. Lipids and reagents

POPG [16:0/18:1-PG, 1-palmitoyl-2-oleoyl-*sn*-glycero-3-phospho-(1′-*rac*-glycerol) sodium salt, no. 840457], DOPG [18:1-(Δ9-*cis*)-PG, 1,2-dioleoyl-*sn*-glycero-3-phospho-(1′-*rac*-glycerol) sodium salt, no. 840475], POPC [16:0/18:1-PC, 1-palmitoyl-2-oleoyl-*sn*-glycero-3-phosphocholine no. 850457], DOPC [18:1-(Δ9-*cis*)-PC, 1,2-Dioleoyl-*sn*-glycero-3-phosphocholine no. 850375], and PC [L-α-phosphatidylcholine, egg, chicken, no. 840051] were purchased from Avanti Polar Lipids (Alabaster, AL, USA). IP3 [D-*myo*-inositol-1,2,6-trisphosphate sodium salt, no. 10007780] and PIP2 [1-(1,2R-dihexadecanoyl-phosphatidyl) inositol 3,5-bisphosphate, trisodium salt, no. 10008398] were products from Cayman Europe (Tallinn, Estonia). N-(7-nitrobenz-2-oxa-1,3-diazol-4-yl)−1,2-dihexadecanoyl-*sn*-glycero-3-phosphoethanolamine (NBD-PE) and Lissamine™ rhodamine B 1,2-dihexadecanoyl-*sn*-glycero-3-phosphoethanolamine (Rh-DHPE) were from Invitrogen™, Molecular Probes (Eugene, OR, USA).

For *in vitro* experiments, IP3 was dissolved in *A.dest* (AD) and PIP2 in PBS. Phospholipids were dissolved in chloroform, followed by evaporation under a stream of nitrogen. To form small unilamellar vesicles, PBS was added and the vial was put in an ultrasound bath for 30 min, followed by a temperature cycle comprised of 3x alternating between 4 °C and 60 °C for 30 min each. Lipid stocks were stored at 4 °C over night prior to use.

The poractant alfa preparation Curosurf® was a kind gift from Chiesi (Parma, Italy), ATP and LPS (*E. coli* serotype O127:B8, L5668) were obtained from Sigma Aldrich (St. Louis, MO). For lipid extraction and lipidomics, all chemicals and solvents were purchased in the highest available purity. Methanol, water and 2-propanol were purchased from Fluka (Buchs, Switzerland) in LC-MS grade. Chloroform (stabilized with ethanol), acetyl chloride, tetraethyl ammonium chloride and triheptadecanonate (TAG 51:0) were purchased from Sigma-Aldrich (Munich, Germany). All other lipid standards were purchased from Avanti Polar Lipids (Alabaster, AL, USA).

2.2. Activation of human macrophages

Human monocytes were isolated from peripheral blood of healthy volunteers. The procedure was approved by the Ethics Commission of the University of Lübeck. Volunteers had given their informed consent. Heparinized blood was separated with a Hypaque-Ficoll gradient (Biochrom, Berlin, Germany), monocytes were collected, washed twice in HANKS medium and resuspended in RPMI 1640 medium supplemented with 4% human AB-serum, 100 U/ml penicillin, 100 μg/ml streptomycin, 2 mM L-glutamine and human monocyte colony stimulating factor, and cultured for 7 d in teflon bags (American Fluoroseal Corp., Gaithersburg, MD, USA) at 37 °C and 5% CO_2. Subsequently, the macrophages were harvested, and washed twice with RPMI 1640.

Primary lung macrophages were isolated from tumor-free lung tissues from surgical specimens of patients who underwent pneumectomy or lobectomy at the LungenClinic Großhansdorf. The use of patient lungs for research purposes was positively reviewed by the ethics committee at the University of Luebeck (statement no. 07–157 and 14–043). Lung tissues were used for isolation of alveolar macrophages as part of a protocol for the isolation of alveolar epithelial cells type II (Marwitz et al., 2016). Fresh lung tissues were rinsed in sterile PBS to remove excess blood and stored in RPMI 1640 (Life Technologies) supplemented with 10% FCS and 1% penicillin/streptomycin at 4 °C until further use. The tissues were manually dissected using surgical razors and rinsed in

AECII buffer (1.9 mM calcium chloride dihydrate; 1.3 mM magnesium sulfate heptahydrate; 136 mM sodium chloride; 6.1 mM potassium chloride; 3.2 mM disodium hydrogen phosphate; 6.1 mM glucose and 9.9 mM HEPES) using a sieve to remove residual blood. Dissociation was achieved by incubation at 37 °C and 5% CO_2 in AECII buffer supplemented with 2 mg/ml Dispase II (Roche Applied Sciences, Mannheim, Germany) for 60 min under constant stirring. Tissue pieces were further filtered through nylon gaze of decreasing pore size (100 μm, 50 μm, 20 μm) und finally sedimented for 15 min at 478 rcf at room temperature. The cell pellets have been resuspended in 50 ml AECII buffer supplemented with 0.001% Accutase (MilliPore, Darmstadt, Germany) (v/v) and 20 μg/ml DNAse I (Roche Applied Sciences, Mannheim, Germany). These suspensions were applied in 10 ml portions onto 10 ml Biocoll gradient solution (Biochrome) and centrifuged for 25 min at 478 rcf. The resulting interphase was washed with AECII buffer at 478 rcf for 15 min at 4 °C and resuspended in cell culture medium. Cells were seeded in 5×10^7 portions on 6 cm petri dishes and incubated for 20 min at 37 °C in an incubator to allow for adherence of alveolar macrophages. Non-adherent cells were removed and used for isolation of alveolar epithelial cells type II, while the adhered macrophages were further used in this study.

For cell stimulation experiments, macrophages were seeded at 1×10^5 cells/well in serum-free Opti-MEM Gibco (Thermo Fisher Scientific, Waltham, MA, USA) and incubated at 37 °C, 5% CO_2 for 1 h to allow adherence. POPG, DOPG, IP3, PIP2, or control lipids were added at the indicated concentrations and incubated for 30 min at 37 °C. Subsequently, cells were stimulated with 10 ng/ml LPS and cells were incubated for 4 h. Cell free supernatant samples were taken for the analysis of TNF-α production. For the analysis of IL-1β production, cells were further incubated for 19 h. Subsequently, 5 mM ATP was added and cells were incubated for 1 h to induce inflammasome activation. 4 h- and 24 h-supernatants were analyzed by human TNF ELISA set (BD Biosciences, San Jose, CA, USA) and human IL-1β/IL-1F2 Duoset (R&D Systems, Wiesbaden, Germany).

2.3. Surfactant therapy of neonatal ARDS in piglets

The experimental scheme of the triple hit nARDS model was approved and registered by the committee on animal protection for the federal state of Schleswig-Holstein and is described in detail in Spengler et al. (Spengler et al., 2018). Neonatal ARDS was induced in newborn piglets by 1. repeated airway lavage to mimic the reduced surfactant amounts in lungs of newborns suffering from nARDS, 2. artificial overventilation to induce tissue disruption and ventilation stress, and 3. LPS-installation into the lungs to mimic infection with Gram-negative bacteria. Piglets were continuously monitored and obtained intensive care during the course of the experiment. The assignment of the treatment groups is outlined in Table 1. Surfactant was applied three times at 2 h, 26 h, and 50 h. For this, Curosurf® was diluted in 0.9% saline to 20 mg/ml for surfactant therapy. Piglets received 50 mg/kg (as an average, 125 mg total in 6.5 ml) Curosurf® by intratracheal instillation. For Curosurf® enrichment, IP3 (in *A.dest*) and PIP2 (in PBS) were prepared at 2.5 mg/ml. POPG and DOPG were prepared at 7.5 mg/ml in PBS and 1 ml of these preparations was added to 6.5 ml Curosurf® directly before installation into the lungs. The final concentrations of supplemented compounds in Curosurf® were calculated to be 709.5 μM IP3, 332.5 μM PIP2, 1342 μM POPG, and 1298 μM DOPG, respectively. Given an average functional residual capacity of ~15 ml/kg following repeated airway lavage, the theoretical endobronchial concentrations of the intervention substances were IP3 339 μM, PIP2 159 μM, POPG 258 μM, and DOPG 250 μM. For biophysical measurements, similar ratios of Curosurf® and IP3, PIP2, POPG, and DOPG were prepared at the final concentrations required for the experiments.

Table 1
Treatment groups of the nARDS study.

Group	Treatment
Control (C)	no surfactant therapy (air bolus)
S50	Curosurf® (50 mg/kg)
IP3	Curosurf® + IP3
PIP2	Curosurf® + PIP2
POPG	Curosurf® + POPG
DOPG	Curosurf® + DOPG

2.4. Size and zeta-potential measurements

The phospholipid preparations that were used for the supplementation of Curosurf® were characterized by determining their size and the zeta surface potential. For this, 5μl phospholipid liposomes in PBS were added to 45μl PBS, mixed, and diluted to a final volume of 1 ml in *A. dest*. The size of liposomes was measured on a ZetaSizer Nano device (Malvern Instruments, Kassel, Germany) by dynamic light scattering at 25 °C. Samples were equilibrated for 3 min to 25 °C and subsequently the liposome size was determined by triplicate measurements for each sample in three independent experiments. The zeta-potentials of phospholipid liposomes were determined by measuring the velocity (v) of the liposomes in a driving electric field with an effective voltage of 152 V via dynamic light scattering at 25 °C. The corresponding electrophoretic mobilities (v/E) were calculated and the associated zeta-potentials were calculated using the Smulochowski approximation. The data represent the means and SD of $n = 3$ independent experiments.

2.5. Förster-resonance-energy transfer (FRET)-spectroscopy

The mixing/integration of phospholipid liposomes with Curosurf® was analyzed exemplarily for liposomes made from POPG and DOPG. For this, the phospholipid liposomes were labeled with *NBD-PE (donor) and *Rh-DHPE (acceptor) dyes at 100:1:1 M. Liposomes were diluted in PBS to a concentration of 10 μM and equilibrated to 37 °C. Measurements were performed on a Fluorolog-3 (Jobin Yvon Inc., Edison, NJ, USA) under constant stirring. The fluorescence intensities I_{Donor} and $I_{Acceptor}$ were adjusted to equal intensities (ratio = 1) before the measurement and recorded for 50 s to obtain the baseline signal. At t = 50 s, Curosurf® at 20 mg/ml in NaCl was added to obtain a final surfactant to phospholipid ratio according to the supplemented Curosurf® preparations and signals were recorded for another 250 s. The ratios $I_{Donor}/I_{Acceptor}$ were calculated, with a ratio >1 indicating an increase in liposomal membrane surface area by integration/mixing of the liposomes with the Curosurf® surfactant.

2.6. Fourier-transform infrared spectroscopy (FT-IR)

Fluidity and phase-transition of lipids was determined by infrared spectroscopy carried out with an IFS-55 spectrometer (Bruker, Billerica, MA, USA). Curosurf® preparations were prepared according to the preparations in the piglet model stated above to a final concentration of 40 mg/ml. Samples were placed between CaF_2 crystals and cooled to 4 °C. Temperature scans were performed automatically between 10 °C and 70 °C with a heating rate of 0.6 °C min^{-1}. Every 3 °C, 65 interferograms were accumulated, apodized, Fourier-transformed and converted to absorbance spectra. The main vibrational band used for the evaluation of the gel to liquid phase transition of the lipids was the symmetrical stretching vibration of the methylene groups ν_s (CH_2) located around 2852 cm^{-1} The phase transition temperature (T_c) between the ordered β-phase and the fluid α-phase was determined as the temperature of the inflection point of the peak absorption wavenumber.

2.7. Small-angle X-ray scattering (SAXS)

SAXS experiments of surfactant were performed at the BioSAXS beamline P12 of the European Molecular Biology Laboratory (EMBL) at

the synchrotron light source PETRA III at DESY (Hamburg, Germany). For SAXS measurements, Curosurf® samples were prepared to a final lipid concentration of 40 mg/ml and were placed in 80 mm long 1 mm thick glas capillaries (Hilgenberger GmbH, Malsfeld, Germany) in an automatically xy-adjustable capillary sample holder with temperature control. Diffraction experiments were performed with 0.04 s exposure time and 20 frames per sample were averaged. Diffraction was detected on a 2D photon counting Pilatus 2 M detector calibrated with silver behenate. Scattering patterns were investigated in the range of the scattering vector $0.1 < s < 1.0\ nm^{-1}$ ($s = 2 \sin \theta/\lambda$, 2θ scattering angle and $\lambda = 0.124$ nm) and were recorded in dependence of temperature between 20 °C and 80 °C. The scattering patterns were evaluated by assigning the spacing ratios of the main scattering maxima to defined three-dimensional structures (Luzzati and Husson, 1962; Luzzati et al., 1993). The lamellar structures are most relevant here. They are characterized by reflections grouped in equidistant ratios, *i.e.*, 1, 1/2, 1/3, 1/4, etc. of the lamellar repeat distance d_l.

2.8. Surface tension measurements

Static and dynamic surface tension was determined with a pulsating bubble surfactometer (PBS; Electronetics Corp. New York, NY). For this, Curosurf® was diluted to 20 mg/ml in 0.9% NaCl and compounds or buffer control (0.9% NaCl or *A. dest*, AD in the case of IP3) were added according to the fortified surfactant preparations in the piglet model stated above. Samples were further diluted to 2 and 2.5 mg/ml in 0.9% NaCl and incubated for 30 min at 37 °C under gentle agitation before measurement. An air bubble was generated at a radius of 0.4 mm using microscopic calibration in a sample chamber containing approximately 42µl of the surfactant preparations by aspirating ambient air through a chimney. After 30 s, the PBS was started by recording the transmural pressure between the sample chamber and ambient air during the terminal 10.6 s of adsorption (total period ~ 1 min) and subsequently during dynamic pulsation for 5 min. The bubble was cyclically expanded and compressed (50% of surface area) at a frequency of 20/min and 37 °C. The surface tension (γ) at start, at end of recording of adsorption, during pulsation at maximum (γmax) and minimum (γmin) bubble size was calculated using the Young-Laplace equation.

2.9. Determination of surfactant proteins SP-A and SP-D from bronchoalveolar lavage (BAL)

For surfactant protein A (SP-A) and D (SP-D) determination, BAL samples and human SP-A or SP-D protein controls were separated on 12% Tris-acrylamide gels. The proteins were transferred to nitrocellulose membranes and washed in TBST. Membranes were blocked for 1 h in non-fat dry milk in TBST, incubated at 4 °C overnight with goat anti-human SP-A antibody or goat anti-human SP-D antibody (Santa Cruz, Dallas, TX, USA). HRP-conjugated secondary antibody was added for 2 h at room temperature and analyzed by ECL (Thermo Fisher Scientific, Waltham, MA, USA). Band intensities were quantified using ImageJ 1.45S analysis software (NIH, Bethesda, MD, USA) and normalized to the respective SP-A or SP-D protein controls.

2.10. Lipid extraction from bronchoalveolar-lavage derived surfactant

Surfactant samples from piglets were obtained at time point 0 h from the first pulmonary lavage and at time point 72 h at the end of the experiment by instillation of 30 ml/kg warm 0.9% NaCl. Volumes of the bronchoalveolar lavages (BAL) recovered from the lungs were in the range of 73%. BAL was processed by the addition of the cOmplete EDTA-free anti-protease cocktail (Roche; 200µl/10 ml BALF) and centrifuged for 10 min at 1500 rpm to sediment the cell fraction. Surfactant was harvested from the top of the supernatant, snap frozen in dry ice and stored at −80 °C. Cell- and surfactant-free lavage fluid was stored at −20 °C.

Surfactant lipids were extracted in a batch procedure including $n = 84$ surfactant samples to provide comparable conditions for all samples. Extraction was performed from 10µl of surfactant samples according to the protocol of Bligh and Dyer (Bligh and Dyer, 1959). The composition of the poractant alpha used in the experiments was determined from an extract of 10µl Curosurf® and 10µL 0.9% NaCl in quadruplicates. Blank extraction samples, containing 10µl LC-MS grade water instead of surfactant were processed in the same manner as all other samples for quality control. 0.5µl of a butyl hydroxy toluene solution (1 mg/ml in methanol) were added to each sample. Afterwards, 5µl of an internal standard mix (Supplemental information, Table S1) were spiked into the samples. Each sample was mixed with 320µl chloroform and 640µl methanol containing 3% acetic acid and the mixtures were incubated for 30 min at room temperature. Afterwards, 320µl water were added to induce phase separation and the samples were incubated again for 30 min while continuous shaking. The samples were centrifuged for 15 min at 3700 g. The lower, organic, phase was transferred into a separate collection tube and the water phase was re-extracted with 320µl chloroform. After incubation for 30 min with continuous shaking, the samples were centrifuged, again, and the lower phase was collected and combined with the extracts from the first extraction step. The extracts were concentrated in a vacuum centrifuge until complete dryness and resolved on 100µl of chloroform/methanol/water (60/30/4.5; v/v/v). Samples were stored at −80 °C until mass spectrometric analysis.

2.11. Mass spectrometric lipid analysis

Lipid extracts were diluted 1:100 in chloroform/methanol/iso-propanol (1:2:4; v/v/v) containing 0.05 mM tetraethyl ammonium chloride. Samples were analyzed using automated flow-injection on a Q Exactive Plus Mass Spectrometer (Thermo Scientific, Bremen, Germany) equipped with a 1100 series HPLC system (Agilent Technologies, Waldbronn, Germany). Ten microliters sample volume were injected (injection speed 10µl/min) into an isocratic flow of chloroform/methanol/iso-propanol (1:2:4; v/v/v) containing 0.05 mM tetraethyl ammonium chloride with a flow rate of 10µl/min. Survey MS scans were acquired for 5 min in a mass range from *m/z* 350 to 1200 with a mass resolution of 280,000 at *m/z* 200. Capillary voltage was set to 3.7 kV in negative and to 4.3 kV in positive ion mode. Source temperature was 210 °C and S-lens RF level was set to 100%. Four injections were performed per sample: twice positive and negative ion mode in separate runs. In sum each sample was analyzed for 30 min.

2.12. Quantification of free cholesterol

Free cholesterol was quantified using derivatization with acetyl chloride as described earlier by Liebisch et al. (Liebisch et al., 2006). Briefly, 10µl of the crude lipid extracts were derivatized, dried and afterwards resolved in 100µl chloroform/methanol/water (60/30/4.5; v/v/v). Derivatized samples were analysed by automated flow injection on a Q-TOF Ultima quadrupole time-of-flight mass spectrometer (Waters, Milford, USA) coupled to a 1100 Series HPLC-system (Agilent, Waldbronn, Germany) using choroform/methanol/2-propanol (1:2:4; v/v/v) containing 3.7 mM ammonium acetate as eluent. 1µl sample was injected into an isocratic flow of 8µl/min (0–2.5 min post injection) and 20µl/min (2.51–4.5 min post injection) with and equilibration before the next run with 8µl/min (4.51–5 min post injection). The mass spectrometric acquisition consisted of two scans over the complete run time: (1) MS/MS scan (product ion scan) of precursor ions *m/z* 446.4 (cholesterol acetyl ester) and (2) MS/MS scan (product ion scan) at *m/z* 453.4 (cholesterol-d7 acetyl ester). QuanLynx module (MassLynx 4.0, Waters) was used for quantification. Quantification was applied on CID-transitions *m/z* 446/369 (cholesterol) and *m/z* 453/376 (cholesterol-d7) by integration of the flow-injection peak. Linear quantification was achieved by referring the cholesterol signal to cholesterol-d7.

2.13. Lipid identification and quantification

LipidXplorer software (Version 1.2.6) was utilized to search for the lipid classes: SM, LPS, PS, LPG, PG, LPE, PE, PE-O, PA, LPC, PC, PC-O, LPI, PI, CL, Cer and HexCer using customized MFQL-scripts (Herzog et al., 2011). Lipids were only assigned to a mass spectrometric signal when the mass error for a match was below 2 ppm. The dataset was manually corrected for overlapping lipids (isobaric species), isotopic pattern and all ambiguous lipid identifications were removed. Interfering signals from the sample matrix were removed by comparing the average intensity of matching mass spectrometric signals in blank-extract-measurements and surfactant samples. Each lipid species whose abundance in surfactant extracts was lower than ten-fold of the intensity in average blank measurements was removed. Lipids species were quantified based on corresponding internal standard of the same lipid class (Supplemental information, table S1) and are expressed in pmol/µl surfactant. For lipid classes without internal standard, quantities were determined in relation to the sum-intensity of internal standards (LPC, SM, PC, PE and TAG in positive ion mode; LPC, PA, PC, PG, PS and PE in negative ion mode), thus reflecting a relative concentration (Graessler et al., 2009). Mean values for one sample were determined from 4 technical replicates. Afterwards, individual results for positive and negative ion mode were aligned. Lipid species were annotated as follows: Lipid Class [No. of carbon atoms in side chains: No. of unsaturations in side chains]. For sphingolipids: Class [No. of carbon atoms in side chains: No. of unsaturations in side chains; No. of hydroxylations]. PE-O/PC-O: Lipid species with one alkyl linked side chain instead of acyl link.

2.14. Statistical data analysis

2.14.1. Data normalization

For statistical data analysis the 'relative abundance (%)' was calculated by division of each lipid quantity by the sum of all lipid quantities in a sample.

2.14.2. Data filtering

Before data analysis, four samples with the lowest number of identified lipids (F29_DOPG, F43_Control, F65_POPG, F68_S50) and four samples with the highest number of identified lipids (F22_0 h, F50_PIP2, F66_0 h, F69_PIP2) were removed from the dataset. In the consecutive analysis only lipid species were further considered that were detected in at least 80% of the remaining samples.

2.14.3. Hierarchical clustering

Hierarchical clustering was computed with GeneCluster 3.0 (de Hoon et al., 2004) and visualized with JavaTreeView 1.1.6r4 (Saldanha, 2004). Pure Curosurf® extracts and 72 h control samples without intervention were not considered in this analysis. In GeneCluster the dataset of relative abundances was log2-transformed and the lipid species were mean-centered. Only lipid species with an overall standard deviation higher than 0.1 in the dataset were considered for clustering. Hierarchical clustering was calculated for individual samples as well as for lipids using Euclidean Distance metric and Complete Linkage clustering method. In JavaTreeView the pixel contrast was set to 1. Clustering of 72 h samples was performed in the same manner with the exception that exclusively 72 h samples were considered.

2.14.4. Statistical analysis

Two-way ANOVA was calculated with GraphPad Prism (Versions 5 and 6, GraphPad software Inc.). Significance was assumed with a $p < 0.05$.

3. Results

3.1. Inflammasome activation in human macrophages is reduced by anionic phospholipids

To evaluate the capacity of phospholipids to attenuate cellular activation, we analyzed a set of synthetic phospholipids with negative head group charge (PIP2, the head group derivative IP3, POPG, and DOPG) with respect to their capacity to inhibit the cytokine response of human macrophages to bacterial LPS as a stimulus mimicking bacterial infection in nARDS. The canonical inflammasome pathway was activated in a sequential protocol providing LPS challenge as signal 1 and ATP challenge as signal 2. Pretreatment of monocyte-derived macrophages with phospholipids led to significant inhibition of IL-1β production by PIP2, POPG, and DOPG in a dose-dependent manner (Fig. 1A). Also TNF-α production was potently blocked (Fig. 1B), confirming previously published data (Kuronuma et al., 2009). In contrast, IP3 did not confer any inhibition of IL-1β and TNF-α production (Fig. 1A, B). Determination of the IC50 concentrations revealed PIP2 as the strongest inhibitor for both cytokines (2.6 µM for IL-1β and 0.62 µM for TNF-α), IC 50 values for POPG and DOPG were higher by factors 2–10 (Fig. 1C). Of note, IC50

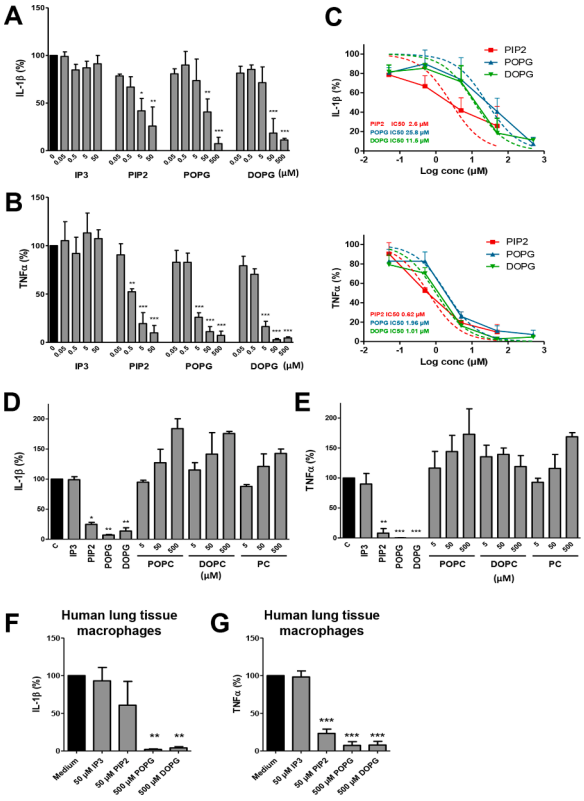

Fig. 1. Phospholipids with anionic, but not with neutral headgroups inhibit inflammatory activation of human macrophages by LPS. (A) IL-1β and (B) TNF-α production by human monocyte-derived macrophages stimulated with 10 ng/ml LPS and treated with increasing concentrations of the intervention substances for 4 h (TNF-α production) or for 23 h followed by 5 mM ATP for 1 h (IL-1β production). Cytokines were determined from cell-free supernatants. Values are means ± SEM of 4 independent experiments with cells from individual donors. (C) IC 50 values were determined from log transformed data sets. (D) IL-1β and (E) TNF-α production by human monocyte-derived macrophages stimulated as stated above in the presence of neutral phospholipids. Values are means ± SEM of 3 independent experiments. (F) IL-1β and (G) TNF-α production by lung tissue macrophages stimulated as stated above. Values are means ± SEM of 3 independent experiments. Differences between the groups (* $p<0.05$, ** $p<0.01$, *** $p<0.001$) by one-way ANOVA for LPS+PIP2/POPG/DOPG.

values also demonstrate that the inhibition of IL-1β production by phospholipids was an order of magnitude less sensitive than inhibition of TNF-α production. To investigate the specificity of phospholipids, we analyzed a set of control phospholipids with comparable fatty acid composition but neutral head group charge at physiological conditions, 16:0/18:1 phosphatidylcholine (POPC) and 18:1-(Δ9-*cis*)-phosphatidylcholine (DOPC), and also a natural mixture of phosphatidylcholine (PC). These PC molecules did not inhibit IL-1β and TNF-α, demonstrating a strict specificity of the inhibitory effect on the lipid head group (Fig. 1D, E).

Macrophage populations represent a complex pool of specialized immune cells with highly adapted immune functions fitting to the requirements of different organs (Murray and Wynn, 2011). Alveolar macrophages are the primary resident immune cells in the lung. Their activation is tightly controlled at different levels to maintain immune homeostasis (Minutti et al., 2017; Moulakakis et al., 2007; Sender et al., 2013). To gain information on the inhibition profile of primary lung cells, macrophages were isolated from the lungs of patients undergoing pneumonectomy. In these cells, stimulation of IL-1β by LPS and ATP was significantly reduced by POPG and DOPG and partially reduced, but not statistically significant by PIP2 (Fig. 1F). Again, inhibitory effects on TNF-α secretion were more pronounced (Fig. 1G).

Of note, IP3 did not exhibit any inhibitory effects on IL-1β and TNF-α production in monocyte derived- and primary tissue macrophages, suggesting that negative head group charge alone is not sufficient to directly modulate macrophage activation, but a hydrophobic molecular component is required in addition (Fig. 1A-G). These results demonstrate that anionic phospholipids provide efficient inhibition of inflammatory mediators in LPS-stimulated macrophages and might thus support a balance towards lung homeostasis.

3.2. *Biophysical characterization of phospholipid fortified surfactant*

In a next step the clinical approved surfactant preparation Curosurf® was enriched by addition of IP3, PIP2, POPG or DOPG and biophysical characterization was performed to obtain fundamental information on physical surfactant properties. Characterization of the phospholipid liposomes (IP3, POPG, DOPG) by light scattering showed small liposomes with a size range of 139.8 ± 2.1 nm for PIP2, 257.7 ± 23.5 nm for DOPG, and 229.8 ± 7.1 nm for POPG (Fig. 2A). As expected, all three lipids had a negative zeta potential with decreasing negative values in the sequence PIP2 −52.1 ± 4.9 mV, DOPG −73.9 ± 3.6 mV, and POPG −82.58 ± 1.7 mV (Fig. 2B). Exemplarily performed FRET-analysis of fluorophore-labeled phospholipid liposomes showed that the liposomes rapidly admix with the Curosurf® surfactant as can be taken from the increase in fluorescence ratio of the FRET-donor and acceptor dye (Fig. 2C), but not with protein-free pure DPPC liposomes (data not shown). The fluidity state of lipids is an important physico-chemical characteristic determining the behavior of membranes. At low ambient temperatures the acyl chains are in a solid gel (β)-phase characterized by low fluidity of the acyl chains. At higher temperatures the acyl chains are in a liquid-crystalline (α)-phase with high fluidity of the hydrocarbon chains. The main gel to liquid-crystalline phase transition occurs at a characteristic phase transition temperature T_c.

Curosurf® showed a clear and defined phase transition at 37.1 °C. Addition of IP3, PIP2, did not affect the phase behavior, POPG and DOPG slightly reduced the phase transition temperature to 34.5 °C and 36.0 °C, respectively (Fig. 2D). To gain insights into the membrane organization, surfactant preparations were analyzed by small-angle X-Ray scattering (Fig. 2E). At 20 °C Curosurf® control (+PBS) showed sharp diffraction peaks indicative of highly hydrated coordinated membrane layers. The equidistant spacing of diffraction maxima at d_1 (11.90 nm), $d_1/2$ (5.84 nm), $d_1/3$ (3.92 nm) and $d_1/4$ (2.98 nm) are indicative of an L_α phase with multilamellar membrane organization and a lamellar repeat distance (d-spacing) of 11.90 nm of a membrane bilayer including the hydration layer. Between 35 °C and 40 °C a phase transition occurs, as can be taken from the broadening of the peak, indicating a lower coordination of membrane stacks, and a decrease in the membrane d-spacing to 10.50 nm due to melting of the acyl chains. PIP2 decreased the d-spacing at 20 °C from 11.90 nm to 11.56 nm. The addition of POPG and DOPG to Curosurf® decreased the d-spacing to 11.30 nm and 11.36 nm, respectively, and both phospholipids induced the occurrence of a beginning non-lamellar phase at 35 °C and above (reflections indicated by arrows). Control measurements were also performed on Curosurf® diluted in saline (+NaCl), to analyze effects of IP3. Curosurf® +NaCl showed a dominant first order diffraction peak at 7.94 nm. The peak spacing d_1 (7.94 nm), $d_1/2$ (3.97 nm) is indicative of a lamellar L_α-phase. Further reflections indicate the existence of a second surfactant phase. The addition of IP3 induced the appearance of a new major diffraction peak at 11.24 nm showing enlargement of the lamellar repeat distance of the L_α phase. No phase transition was observed in the presence of IP3, instead, above 35 °C the major peak shifted to 7.75 nm, showing that the non-lipophilic inositol compound clearly exhibits effects on the organization of the surfactant membranes (Fig. 2E).

The biophysical function of the diluted surfactant was evaluated by surface tension measurements. Static surface tension at start and end adsorption of samples at 2 and 2.5 mg/ml showed a good biophysical activity with mean surface tensions below 30 mN/m. Using preparations of 2 mg/ml phospholipids at start of adsorption, a significantly increased surface tension was found in samples containing PIP2 (28.2 ± 3.1 N/m; mean ± SD) compared to the control (NaCl-control: 26.8 ± 0.8 mN/m; Fig. 2F, $p<0.05$). With exception of this, no differences between Curosurf® (2 or 2.5 mg/ml) diluted in saline and Curosurf® plus PIP2, POPG or DOPG either at start or end adsorption were found (Fig. 2F).

The time dependent effects of maximum surface tension (γ_{max}) shows relatively stable results for Curosurf® NaCl-control, Curosurf® plus POPG at 2 and 2.5 mg/ml and for Curosurf® plus DOPG at 2.5 mg/ml (Fig. 2G, upper panel). γ_{max} was not stable and increases by time in Curosurf® plus *A. dest* (AD-control) and Curosurf® plus IP3 at 2 and 2.5 mg/ml phospholipids and Curosurf® plus DOPG at 2 mg/ml phospholipids ($p<0.0001$ vs NaCl-control at 300 s, Fig. 2G, upper panel). The most distinct differences in γ_{max} was found between PIP2 containing samples and Curosurf® controls at 2 and at 2.5 mg/ml phospholipids: γ_{max} was increased independently from pulsation length to mean ranges of 48.4–57.6 mN/m (2 mg/ml) or 54.5–59.7 mN/m (2.5 mg/ml) compared to NaCl-control with ranges of 35.3–39.1 mN/m (2 mg/ml) and 32.2–33.6 mN/m (2.5 mg/ml; $p<0.0001$), respectively (Fig. 2G, upper panel; supplemental information, Table S2).

The main biophysical function of lung surfactant is the reduction of the surface tension to values close to zero mN/m during surface area compression, which, in these experiments, is reflected by data on γ_{min} at 50% surface area compression. All preparations showed a time dependent decrease in γ_{min}. During dynamic cyclic compression γ_{min} decreased for all preparations giving finally (after 300 s) non-significant differences compared to controls (Fig. 2G, lower panel). Comparing Curosurf® NaCl-controls with samples plus PIP2, POPG, or DOPG characteristic patterns were found when comparing the time depending decrease of γ_{min}: Fig. 2G demonstrates in comparison to Curosurf® control (NaCl-control) significant differences of γ_{min} for PIP2 ranging from 30 to 180 s, for POPG from 30 to 120 s and for DOPG from 15 (30)–60 s of pulsation. This delay in reduction of γ_{min} is also found by calculating the period until mean-γ_{min} is reduced below the arbitrary value of 10 mN/m. It was 25 s for Curosurf® measurements. After admixture of PIP2, POPG or DOPG this period is delayed to 146, 85, and 65 s respectively.

Samples containing IP3 (in AD) were analyzed separately compared to the respective Curosurf® control (AD-control 2 and 2.5 mg/ml phospholipids). No differences were found in adsorption kinetics. AD-controls showed a time dependent increase of γ_{max} giving maximum values at 300 s of pulsation. This observation is pronounced in the samples containing 2 mg/ml phospholipids. Neither γ_{max}, time

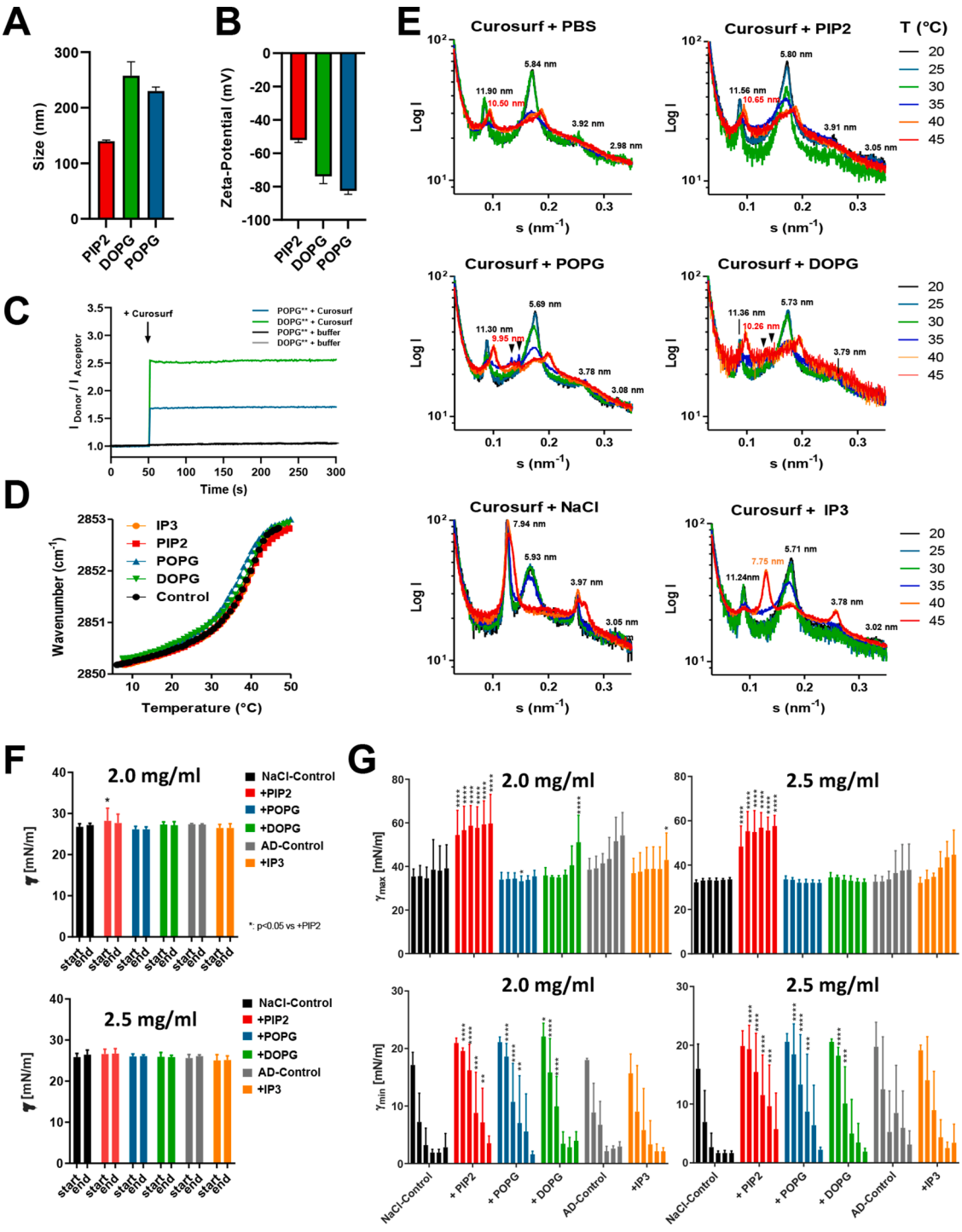

Fig. 2. Biophysical characterization of phospholipid modified surfactant. (A) Size and (B) Zeta-Potential of PIP2, DOPG, and POPG lipid preparations in PBS that were used for the supplementation of Curosurf. Data are mean +SD of 3 independent experiments. (C) Interaction/mixing of fluorophore-labeled POPG and DOPG liposomes (**) with Curosurf® was determined by FRET-Assay. Curosurf was added at $t = 50$ s to the liposomes. Data are mean of $n = 3$ experiments. (D) Acyl chain mobility of Curosurf surfactant membranes (Curosurf control, black; Curosurf with addition of the indicated compounds) in dependence on temperature. Wavenumbers depict the peak position of the infrared-absorption of the symmetric stretching vibration ν_s of the CH_2 groups. Data are representative of 2–3 independent measurements. (E) Nanoscale organization of the Curosurf surfactant membranes was determined by SAXS. Scattering vectors are indicated for temperatures between 20 °C and 80 °C. The spacing of the diffraction maxima is indicted as $d = 1/s$ (nm) in black for 20 °C or in the color code of the respective temperatures. (F) Static surface tension (γ) determined during adsorption at an air bubble at start and end of recording (terminal 10.6 s) determined in the pulsating bubble surfactometer. Results are expressed as mean ± SD of 5 repeated experiments. Sample preparations are Curosurf® (2 or 2.5 mg/ml) diluted in saline plus different lipids (+ PIP2; +POPG; +DOPG; +IP3) or buffer controls (NaCl-control; *A. dest*, AD-control). IP3 required dilution in AD and was compared to AD-control. *: $p< 0.05$ vs. control; Two-way-repeated-measures-ANOVA followed by Tukey's multiple comparison test. (G) Surface tension at maximum (γ_{max}) and minimum (γ_{min}) bubble size recorded in a cyclically 50% compressed bubble in the pulsating bubble surfactometer after 15, 30, 60, 120, 180 and 300 s (left to right in each color group). Sample preparations as described under (F). Results are expressed as mean ± SD of 5 repeated experiments. *: $p < 0.05$, **: $p< 0.01$, ***: $p<0.001$ and ****: $p<0.0001$ vs. control; Two-way-repeated-measures-ANOVA followed by Tukey's multiple comparison test.

dependent reduction of γ_{min}, nor γ_{min} after 300 s values showed differences between Curosurf® or Curosurf® plus IP3 (Fig. 2G; supplemental information, Table S2).

The biophysical studies revealed that surfactant enrichment induced specific changes in the 3D nanoscale organization of surfactant. However, these changes did not impact the biophysically important fluidity state. The functional surfactant activity was changed in terms of increased adsorption, increased maximum and delayed minimum surface tension by PIP2, partly increased γ_{max} and delayed γ_{min} after addition of DOPG and only delayed γ_{min} after addition of POPG. No functional differences were found in samples containing IP3.

3.3. *In vivo evaluation of fortified surfactant in a piglet nARDS model*

In a previous study, the therapeutic effect of the modified Curosurf® was investigated in a porcine model of nARDS. We could demonstrate, that piglets receiving surfactant enriched with PGs and PIs showed improved lung function parameters and reduced tissue destruction. Data on lung performance, clinical measures, tissue inflammatory responses, and lung fibrosis demonstrated significantly reduced pathology (Spengler et al., 2018). In the current part of the study, we focused on the detailed analysis of the lung surfactant composition in the porcine nARDS model, as the composition of lung surfactant is crucial for its biophysical role in breathing, physiological gas exchange and immunological functions. Surfactant samples were obtained from BAL of all piglets at the beginning of the experimental protocol (time point 0 h, $n = 84$) and at the end of the nARDS model (time point 72 h, $n = 6–8$ animals per group). The assignment of the treatment groups is outlined in Table 1.

3.4. *Surfactant lipid profiles of healthy and nARDS piglets: major phospholipid classes*

Lipid profiles of surfactant samples were generated by shotgun lipidomics screens (Schwudke et al., 2007). Surfactant lipids were extracted from surfactant obtained from BAL samples and analyzed by high-resolution mass spectrometry. Lipid species were identified by determining the mass-to-charge ratio (m/z) with an error below 2 ppm and their quantity was estimated on basis of internal lipid standards which were spiked into each sample before the lipid extraction procedure. Data obtained are presented in a way to provide unbiased information on the surfactant composition and insights into the abundance and changes of individual surfactant lipid species and treatment compounds.

First, we focused on delineating the surfactant composition in healthy piglets and piglets with nARDS and compared the lipids obtained from animals at time point 0 h with the lipids obtained from piglets without any therapeutic intervention after 72 h of nARDS (control group). Shotgun lipidomics screens identified a total of 194 different lipid species in the surfactant samples (Supplemental data Table S3). However, because of the severity of the induced pathology, we have dramatically changed efficiencies in collecting surfactant samples between the treatment groups and overall lipid amounts. To be able to focus on the underlying metabolic perturbations, 84 lipids were selected that were present in at least 80% of all samples. These 84 lipids grouped into nine major lipid classes including PC, PI, PE, PS, cholesterol, sphingomyelin, PG, ceramide, and diacylglycerols (DAG). Fig. 3A-C shows significant degradation of total PC, PG and PI after 72 h of nARDS disease progression without therapeutic intervention. Similar results were obtained for all other lipid classes. These data demonstrate a strong overall degradation of pulmonary surfactant lipids during disease progression.

The pulmonary surfactant of healthy and nARDS piglets without treatment was further analyzed for compositional changes regarding the lipid classes. The pie charts in Fig. 3D (0 h) and Fig. 3E (72 h, control group) depict that no major changes in the surfactant lipid profile could

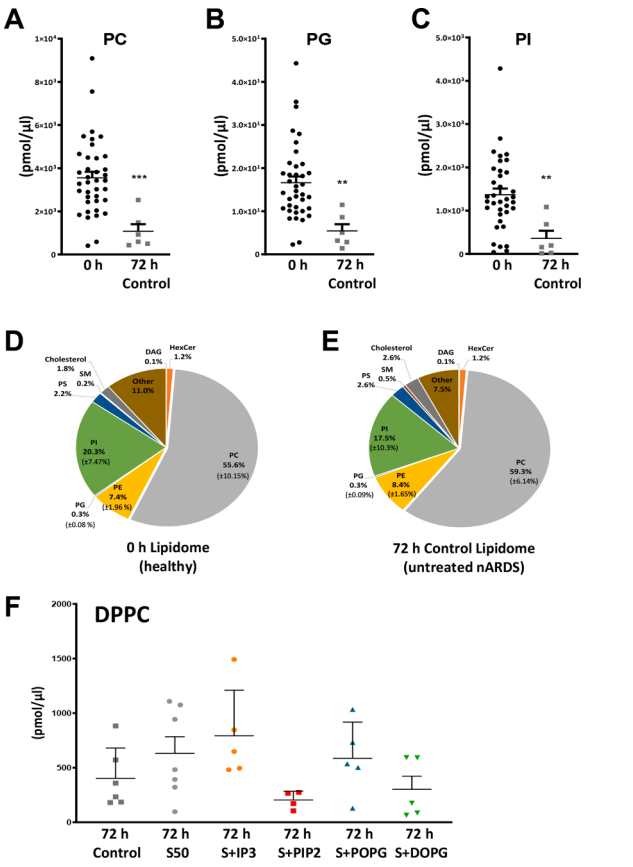

Fig. 3. Piglet pulmonary surfactant is strongly degraded during nARDS progression but the overall lipid composition of surfactant remains stable. (A, B, C) Dot plots displaying abundance of PC, PG, and PI lipid classes (pmol/µl of piglet surfactant sample) of samples at 72 h compared to samples at 0 h. Data are means +SD. Significances were calculated by one-tailed *t*-test (** $p < 0.01$, *** $p < 0.001$). (D) Pie chart of the relative abundances of major lipid classes found in pulmonary surfactant of healthy (0 h) piglets (mean ±SD, $n = 38$). (E) Pie chart of the relative abundances of the major lipid classes found in pulmonary surfactant of untreated nARDS (72 h control) piglets (mean ±SD, $n = 6$). (F) Concentration of DPPC (PC [32:0], (pmol/µl of piglet surfactant sample) in samples at 72 h comparing the treatment groups. Data are mean +SD. Differences between the treatment groups were tested by ANOVA with Dunnett's multiple comparison test and found to be not significant ($p > 0.05$).

be observed after 72 h of untreated disease progression. PC remains the major lipid class. However, the relative abundance of PI species slightly decreased from 20.3% to 17.5%, whereas those of PS, PE, and SM slightly increased (PS: from 2.2% to 2.6%; PE: from 7.4% to 8.4%; SM: from 0.2% to 0.5%; 0 h and 72 h respectively). The PG level remained at its initial very low level of 0.3% (mean value; PG range 0 h, 0.08 - 0.4%; 72 h, 0.19 - 0.4%). Despite the massive reduction in the overall lipid content of the surfactant, the data did not indicate any selective degradation of individual lipid species.

We next compared the untreated control group with the different groups receiving surfactant treatment at time point 72 h of nARDS progression. Surprisingly, we did not observe any significant stabilization of the most abundant surfactant lipid DPPC [PC 32:0] in the surfactant treatment groups (Fig. 3F).

3.5. *Surfactant proteins (SP-A and SP-D) in piglets receiving surfactant therapy*

Surfactant protein (SP)-A and SP-D are the immunologically relevant surfactant proteins with important roles in pathogen recognition and immune response. SP-A is demonstrated to exert strong anti-

inflammatory regulation on alveolar macrophages and represents an important factor in maintaining immune homeostasis. Immune regulation is exerted for example by the direct interaction of SP-A to pathogens or bacterial LPS (Keese et al., 2014; Wright, 2005), interference with LPS transport by the LPS-binding protein LBP (Stamme et al., 2002) and LPS binding to CD-14, TLR4, and MD-2 (Garcia-Verdugo et al., 2005) and by constitutive basal modification of intracellular NF-κB signaling components in alveolar macrophages (Minutti et al., 2017; Moulakakis et al., 2007; Sender et al., 2013). Compared to healthy control piglets before nARDS, a reduction of SP-A was observed after 72 h in all treatment groups, with one exception: IP3 conferred a stabilization of SP-A protein level (Fig. 4A), a fact that could contribute to the anti-inflammatory effects observed in this group (Spengler et al., 2018). We did not observe any significant changes in the levels of SP-D in any of the groups (Fig. 4B). These data are in accordance with previously published findings showing that SP-A is mildly reduced during ARDS in children (Todd et al., 2010).

3.6. Lipid profiles of piglets receiving surfactant therapy

The surfactant lipidomes showed characteristic compositions for the study groups. Hierarchical clustering analysis (Fig. 5) groups the majority of surfactant samples of healthy piglets (0 h) to cluster I (Corr. = 0.727), with only one sample located outside of the cluster. Surfactant samples of the treatment groups were located in cluster II (Corr. = 0.752). All samples of healthy piglets (0 h) were characterized by low abundances of PG species including PG [36:2], PG [34:1], PG [32:0], PG [32:1] and PG [34:2]. The same trend was observed for PE-O [38:5] and SM [34:1] (Fig. 5, bottom). These noted lipids showed the most striking differences between control and treatment and showed highly correlative behavior signified by the clustering (Fig. 5, cluster A, Corr. = 0.549). Lipids comprising long-chain unsaturated acyl moieties, such as PC [38:3], PE [38:4], and PG [36:3], were characteristically increased in the treatment groups (Fig. 5, cluster B). For the majority of PI species, we observed the opposite trend where the relative abundance in 0 h samples was higher when compared to the Curosurf® treatment (Fig. 5, cluster C).

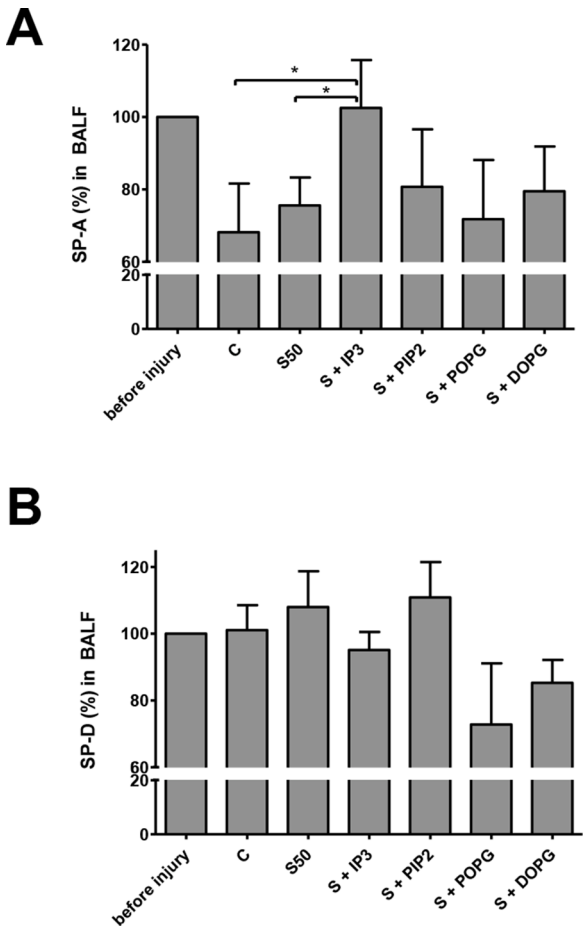

Fig. 4. Immunological active surfactant proteins SP-A and SP-D. (A) SP-A and (B) SP-D protein concentrations in bronchoalveolar lavage samples before lung injury (0 h) and after 72 h of mechanical ventilation. The samples were analyzed in technical duplicates by western-blot and normalized to an internal SP-A/D protein control, as well as to the samples "before injury" (= 100%). Significances were calculated by one-tailed *t*-test (* $p < 0.05$).

The clustering of Curosurf® (Cluster II) treated piglets indicated that some treatment groups have a specific lipidome status when compared to the standard treatment (S50 – gray, Fig. 5). All samples from the DOPG treatment group (DOPG – green, Fig. 5) formed a clearly separated sub-cluster indicating similar lipidome composition. The POPG treatment group was clustered together on the right side of the dendrogram (POPG – blue, Fig. 5) with exception of one sample. All cases of the PIP2 (red, Fig. 5) and IP3 (orange, Fig. 5) treatment groups are found together in subcluster IIa with exception of one PIP2 sample. Furthermore, all lipidomes of IP3 and PIP2 treatment group were located in close proximity to the standard treatment group S50. Nevertheless, it was possible to observe that three of four PIP2 treated samples cluster together.

From the obtained shotgun lipidomics datasets, we assumed that signals of PG [34:1] refer mainly to POPG and signals identified as PG [36:2] mainly to DOPG. We observed an accumulation of PG [34:1] and PG [36:2] in the respective treatment groups which most likely influenced the clustering structure. The utilized analytical workflow did not cover PIP2 and IP3 molecules. However, PI [32:0] was identified as a potential metabolite of PIP2 [32:0] lacking two phosphates and was increased in the PIP2 treatment group. A direct link between IP3 treatment and the overall lipidome composition could not be observed and the IP3 group was clustered together with the S50 group.

3.7. Comparison of the lipidomes of treatment groups with fortified surfactant

In the next step, we performed Analysis of Variance (ANOVA) on the relative abundances (Fig. 6A) and identified significant accumulation of PG [34:1], PG [36:2] and PI [32:0] in the respective treatment groups when compared to the standard treatment S50 with highly significant p-values. This strong accumulation can also be visualized in the group wise comparisons depicted in Fig. 6B. At the same time we compared the overall PG profile of all treatment groups (Supplemental information, Fig. S1) and did not see any effect by treatment additives, except the accumulation of POPG or DOPG, respectively. Additionally, we did not find indications for head group exchange for [34:1] and [36:2] aliphatic chains that were present in the treatment groups. From this perspective, we can conclude that there was no conversion of POPG or DOPG to other lipids covered in this screening such as POPC, DOPC, or the respective PE and PI species. However, we identified a slight but significant ($p < 0.01$) increase of PI [32:0] in the PIP2 32:0 treated surfactants (Fig. 6A, B) where the overall PI composition is not affected in the treatment groups (Supplemental information, Fig. S2).

Next, we aimed at elucidating the effect of the treatment lipids on the surfactant lipidomes. To be able to identify general surfactant alterations in addition to the supplemented treatment lipids, we excluded the lipid species PG [34:1] and PG [36:2] from the analysis. Then, the cut-off for the inclusion of lipid species into the cluster analysis was set to an overall standard deviation (SD) larger than 0.1 to focus the analysis exclusively on species with the highest variability. All 33 lipid components that fulfilled that criteria were further analyzed by hierarchical clustering (Fig. 6C). For the IP3 treatment group we found that 4 of 5 samples clustered together. However, a clear separation of treatment

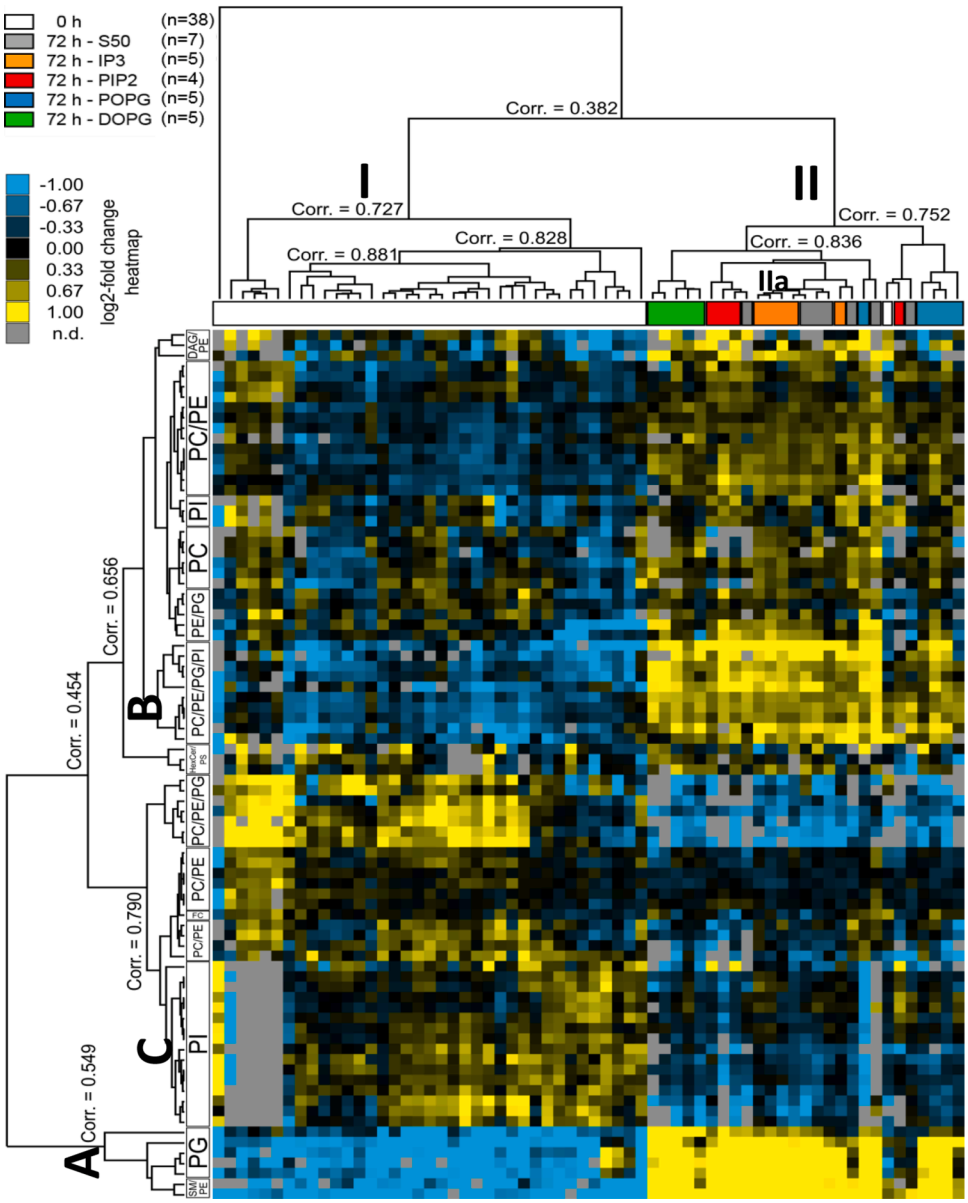

Fig. 5. Lipid profiles of 0 h and 72 h samples are clearly distinguishable. Hierarchical clustering of 64 piglet surfactant samples (tree top). Groups are shown by colored bars above the tree: white, 0 h samples; gray, 72 h Curosurf® (control); orange, 72 h Curosurf® + IP3; red, 72 h Curosurf® + PIP2; blue, 72 h Curosurf® + POPG; green, 72 h Curosurf® + DOPG treatment. 84 lipid species present in 80% of the samples were clustered (tree left). Characteristic lipid species for clusters are noted below the tree. Clustering metric in both cases was 'Euclidean Distance' and method was 'Complete Linkage'. Lipid abundances are expressed on the heat-map as log2-fold changes. Blue coloring expresses a decrease and yellow coloring expresses an increase.

groups from the S50 could not be observed. This result demonstrates that the lipid alterations within the treatment groups were driven by the specific additives while the overall surfactant lipidome was only marginally affected. We conclude that the supplemented lipids accumulate in the lung surfactant without changing the overall lipidome composition and only negligible appearance of conversion products.

4. Discussion

To improve patient care and reduce pathology and mortality in nARDS new treatment options are needed. Among these, improvement of surfactant supplementation therapy represents a promising approach. The current concepts for the development of new generation surfactants are focused on the major phospholipid component of lung surfactant DPPC, the anionic phospholipid POPG and the lipophilic surfactant proteins SP-B and SP-C (Curstedt et al., 2013; Ricci et al., 2017; Sweet et al., 2017). Since several recent papers highlight the involvement of inflammasome activation as a major pathway contributing to the pathophysiology in ARDS (Borthwick, 2016; Grailer et al., 2014; Kolliputi et al., 2012), the current study aimed to (i) address the potential of phospholipids to modulate this pathway, (ii) to analyze the biophysical properties of modified surfactant preparations and (iii) to provide fundamental data on the surfactant composition in the healthy lung, in the diseased lung and under therapy with modified surfactant.

Challenge of macrophages with LPS and ATP is a widely used system to study inflammasome mediated IL-1β production *in vitro*. Our data clearly demonstrate that PIP2, POPG, and DOPG inhibited IL-1β production in monocyte-derived macrophages as well as in primary macrophages from human lung tissue. The IC50 values and doses required for significant inhibition of IL-1ß production were one order of magnitude higher than the doses inhibiting TNF-α production (Fig. 1B, C, E). This difference in the required inhibitory doses is likely due to the different activation pathways involved. The lowest IC50 values were determined for PIP2, IC 50 values for POPG and DOPG were higher by factors 2–10. Clearly, IP3 did not confer any direct inhibiting effect of the IL-1β production in human monocyte-derived and in primary lung macrophages. Similar results were also obtained in experiments on macrophages from piglets (Spengler et al., 2018), underlining that this is a broader species-independent observation.

Inhibitory effects of phospholipids on TLR4 activation by LPS have

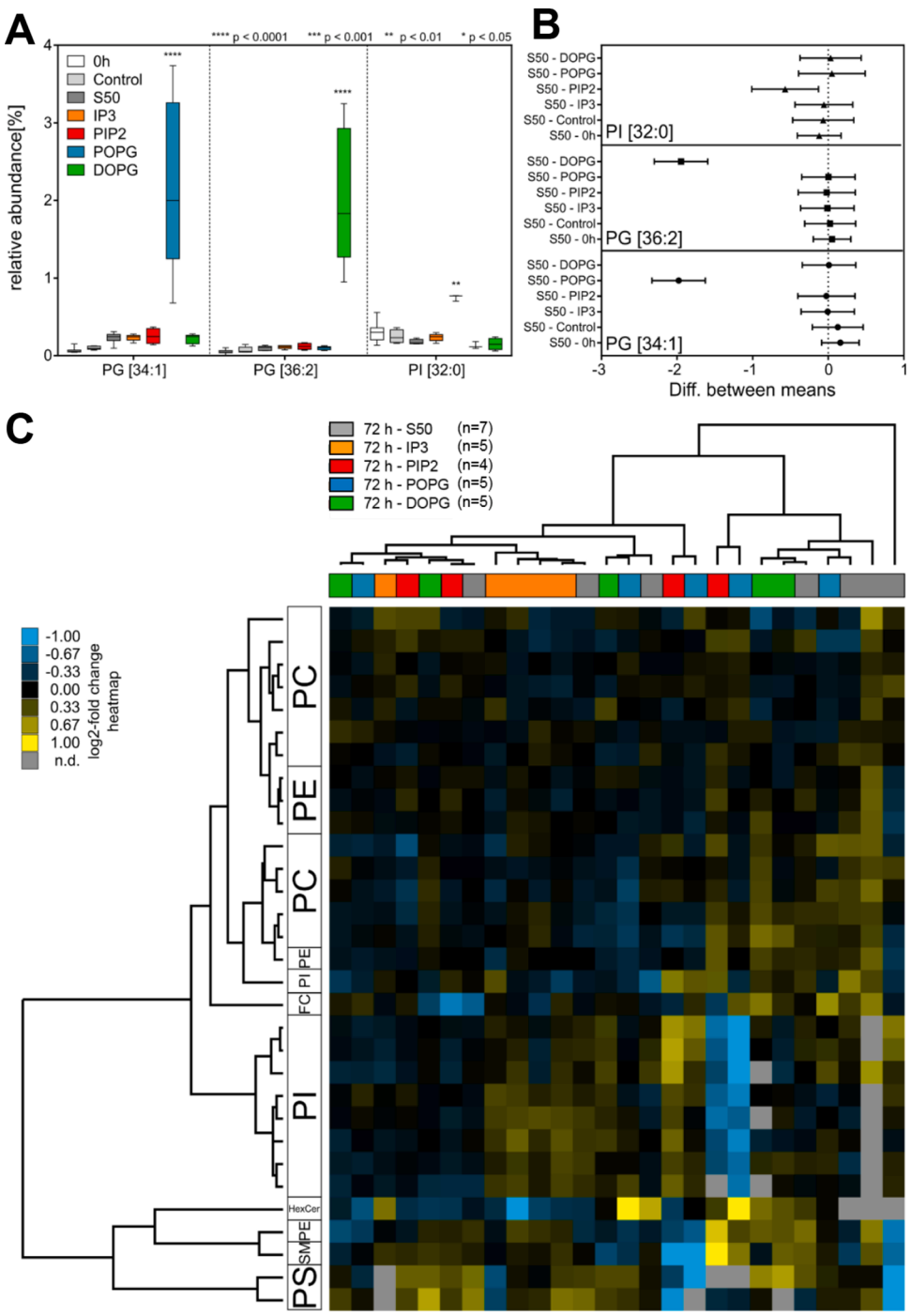

Fig. 6. DOPG and POPG were found accumulated but overall surfactant composition was stable in the model. (A) Box and whiskers plot of PG 34:1, PG 36:2 and PI 32:0. Significant changes were determined by two-way ANOVA and *t*-test with S50 group as control. (B) Mean and 95% confidence intervals for the respective lipid species in all treatment groups. (C) Hierarchical Clustering (GeneCluster 3.0, TreeView) of 72 h samples. Lipid species were filtered according to the overall standard deviation (lower limit 0.1). The heat-map shows log2-fold changes. Clustering was performed using Euclidean Distance and Complete Linkage. The samples were color-coded according to the treatment groups on the upper dendrogram (gray, 72 h Curosurf® (S50, control); orange, 72 h Curosurf® + IP3; red, 72 h Curosurf® + PIP2; blue, 72 h Curosurf® + POPG; green, 72 h Curosurf® + DOPG). The left dendrogram was tagged by lipid classes.

been related to the interaction of anionic phospholipids with several proteins involved in the signaling pathway, including CD14, LBP, TLR4, and MD-2 (Kuronuma et al., 2009; Mueller et al., 2005). POPG and also PI have been shown to be effective inhibitors of TLR4 activation resulting in NF-κB dependent TNF-α release and NO-production (Kuronuma et al., 2009). Efficiency of phospholipid inhibition by POPG has been demonstrated in the context of mycoplasma infection and respiratory viral infections (Kandasamy et al., 2011; Numata et al., 2010, 2012a). So far, the regulatory networks of phospholipid mediated inflammasome activation are not delineated in detail. Not surprisingly, the therapeutic effects of surfactant supplementation observed in our piglet model was much more diverse than would be anticipated from these current *in vitro* studies, reflecting the complex interplay of immune regulation circuits *in vivo*. Piglet groups receiving IP3, PIP2, and POPG modified surfactant showed improvement of vital lung parameters over the observed time course of 72 h, with IP3 and POPG providing the most beneficial effects. With respect to the inflammasome activation pathway, significant inhibition of several steps of the NLRP3-ASC-IL-1β pathway was observed in protein extracts of whole lung tissue for the group receiving IP3, and some effects were evident in the DOPG group (Spengler et al., 2018). Besides the alveolar macrophage, which represents the primary and dominant immune cell in the lung, other pulmonary cell types contribute to the inflammatory scenario. Type II pneumocytes have been shown to respond with inflammasome activation in acute lung injury and ARDS (Kolliputi et al., 2012). The cross-talk and co-stimulatory effects between immune-competent cells and

different stages of regulation should therefore also be considered. In line with this, inhibitory effects of IP3 were observed also on the ceramide axis which might explain the strong effects observed *in vivo*. Furthermore, the potency of IP3 might also not only be a result of local effects, but also of its systemic impact, as immune modulation was not only observed in the lung, but also in the liver (Spengler et al., 2018). To generate a complete picture of the regulatory mechanisms, both types of analysis, on the cellular level as show here and *in vivo* are required.

A study by another group recently demonstrated that the zwitterionic surfactant lipid DPPC can interfere with inflammasome activation by LPS and ATP in the human U937 cell line and in unprimed or LPS-primed human monocytes. In this experimental setting, the authors did not observe inhibitory effects of POPG or PS. They identified nicotinic acetylcholine receptor as target of inhibition by DPPC via modulation of ATP-sensitivity of P2X7 channel gating (Backhaus et al., 2017). This finding represents an interesting new aspect, especially in view of the fact that inflammasome activation pathways in monocytes and macrophages are quite differentially regulated. In our study, the tested neutral PC species mediated even enhanced IL-1β production of macrophages (Fig. 1D). Of note, the neutral lipids alone did not induce TNF-α or IL-1β release and testing of the phospholipid preparations by the Limulus-Amoebocyte Lysate (LAL) assay did not indicate that the enhancing effect is conferred by endotoxin contamination. Together, these observations suggest that also along the axis of inflammasome activation different pathways have evolved to interfere with immune activation and support immune homeostasis in the lung. Within this regulatory network, both the zwitterionic phospholipid DPPC and the anionic lipids contained in the lung surfactant may contribute to provide a well-balanced system.

As changes in the pulmonary surfactant composition have a strong impact on biophysical and physiological lung function, monitoring of the surfactant lipid composition is important for the evaluation of treatment strategies. The comparison of the lipid composition in surfactant of the healthy newborn piglets at $t = 0$ h with the same piglets receiving surfactant therapy after 72 h revealed characteristic changes in the lipid profile of lung surfactant. The typical surfactant profile of newborns dominated by high content of PI species and minor amounts of PG species is reflected in the lipidome data. In ARDS induced by meconium aspiration in newborns, an increased abundance of polyunsaturated lipids was recently reported (Autilio et al., 2020). In line with these data, we observed similar changes in the PC profile of 72 h ARDS untreated controls in comparison to the healthy state ($t = 0$ h). The particular increase of long chain polyunsaturated PC species (PC 36:2, 36:3, 36:4, 38:4, and 38:5) is indicative of cell debris and tissue destruction associated with severe ARDS (Supplemental information, Fig. S3). Upon surfactant treatment, specific lipidome changes were observed. Several lipid species such as PG [34:2], PG [32:0] and PG [32:1] can be identified as components of the Curosurf® preparation used. Especially the increase in PG 34:1 indicates a typical content of POPG contained in the surfactant of adult lungs. However, the overall composition determined in lung surfactant samples from Curosurf® treated piglets represents a unique profile with lipid species that clearly differs from the lipid profile of Curosurf® (Supplemental data Table S3) and (Pelizzi et al., 2002). Several lipid species were identified in the 72 h surfactant samples that were not contained in the surfactant of healthy piglets and not in the Curosurf® preparation. These lipids were mainly PE-ether, however their abundance was quite low. Of note, sampling of lavage and surfactant in different disease states represents a major challenge of this experimental setting. Lipid extraction from lung tissue samples could improve the lipid recovery and quantification of the tissue surfactant pool. The major differences observed were exclusively restricted to the applied lipids, demonstrating that surfactant enrichment resulted in a stable maintenance of the surfactant composition. In line with this, also the immunologically active surfactant proteins SP-A and SP-D were not affected, with the exception of the IP3 group, where SP-A levels were increased, suggesting improved anti-inflammatory regulation by the SP-A route. We initially expected to observe stabilization of the surfactant amounts. However, the data did not indicate significant stabilization of particular and overall lipids in the treatment groups. Nevertheless, we observed significantly improved outcome (Spengler et al., 2018). We conclude that enhancing the amount of surfactant is not the only target to reduce pathophysiology. The immunological effects and the impact of surfactant lipids on cell and tissue metabolism are also of great importance for the outcome. It is therefore of major interest, to obtain more information on the molecule pathways and turnover of surfactant and treatment lipids. Doping of the treatment compounds with lipid tracer could provide such information.

Pulmonary surfactant arranges as a thin film at the air-water interface and in several different types of multilamellar structures. Most peculiar characteristic lipid structures are surfactant lamellar bodies and tetragonal structures named tubular myelin (Perez-Gil, 2008). Systematic investigation into the molecular structure and biophysical behavior of clinical surfactant preparations can provide important information for the development of improved or artificial surfactants. As such, cholesterol, which is usually extracted from clinically used porcine surfactant preparations has recently been demonstrated to have a strong impact on the organization and phase behavior of the porcine surfactant preparations HL-10 (Andersson et al., 2017). The biophysical analysis of the fortified surfactant preparations showed no effects on phase state and fluidity. The SAXS analysis revealed nanoscale modifications of the membrane organization, with a slight reduction of the bilayer d-spacing by the additives. POPG and DOPG induced a tendency to non-lamellar structure at physiological temperature. Of general interest is the observation that the surfactant mesophase differed in saline and in PBS preparations. The much smaller d-spacing of surfactant bilayers observed in saline was strongly increased by IP3, reflecting the strong effects of electric repulsion on membrane organization.

The functional capacity to reduce surface tension *in vitro* were mainly reduced in PIP2 containing surfactant. Also, addition of POPG and DOPG seemed to delay refinement of a surfactant film at the air liquid interface as indicated by delayed reduction of γ_{min} compared to control preparations. To establish a surfactant film with high functional capacity, enrichment of DPPC in the monolayer induced by squeeze- out of non-DPPC components is proposed (Pérez-Gil and Keough, 1998; Xu et al., 2020). This could be in line with the delayed reduction of surface tension during compression of the preparations in the pulsating bubble surfactometer. However after 5 min, no differences in γ_{min} have been found. The functional data derived in the pulsating bubble surfactometer are limited to low surfactant concentrations, since light opacity of higher concentrations avoid proper microscopic adjustment of the bubble size. Concentrations used in this study were close to biophysical inactivation, which *e.g.* is indicated by more stable γ_{max} and γ_{min} results in samples at concentrations of 2.5 compared to 2.0 mg/ml. On the other hand, there are limited data on the physiologic concentration of surfactant in the terminal airways. Of note, as demonstrated in a previous study, the application of the here studied supplemented surfactant preparations conferred improved lung oxygenation in a piglet model, demonstrating sufficient biophysical function of the preparations *in vivo* (Spengler et al., 2018). The described effects on the biophysical function found *in vitro* may be counterbalanced by increasing the phospholipid concentration and/or the concentration of the surfactant proteins-A, -B and/or -C that firstly are known to improve biophysical activity of surfactant and secondly are increased in natural surfactant.

5. Conclusions

In conclusion, our study demonstrates that *in vitro*, PIP2, POPG, and DOPG confer anti-inflammatory immune regulation by inhibiting TNFα and IL-1β release. Enrichment of surfactant resulted in minor modifications of the biophysical state of surfactant. For PIP2 supplementation, the biophysical function to lower the surface tension was impaired. As the anti-inflammatory activity was highest for PIP2, lower

concentrations might be sufficient to retain the physical surfactant function. *In vivo* application of the preparations demonstrated an increased abundance of the treatment compounds with an otherwise stable lung surfactant composition. In conclusion or data show that enrichment with anionic lipids in surfactant therapy is a promising strategy to attenuate hyper-inflammatory responses in pulmonary diseases.

Declaration of Competing Interest

The authors do not have a conflict of interest with the contents of this article to disclose.

Acknowledegements

This project was funded by the Cluster of Excellence Inflammation at Interfaces projects Exc306OTP1 to M.F.K, EXC306OTP4 to A.B.S., and Cluster Laboratory X (lipidomics platform). SAXS Measurements were performed at the EMBL c/o DESY beamline P12 at PETRA III under a beam time grant to A.B.S. We thank Michael Rappolt for his expert advice and supporting data analysis. We acknowledge excellent technical assistance by Irina von Cube, Katja Corrigeux, Chee Keong Tan, Joe Knoof, Verena Scholz, Birte Buske and Gabriele Walter. Curosurf® was kindly provided by Chiesi (Parma, Italy).

Supplementary materials

Supplementary material associated with this article can be found, in the online version, at doi:10.1016/j.ejps.2022.106216.

References

Akashi, S., Ogata, H., Kirikae, F., Kirikae, T., Kawasaki, K., Nishijima, M., Shimazu, R., Nagai, Y., Fukudome, K., Kimoto, M., Miyake, K., 2000. Regulatory roles for CD14 and phosphatidylinositol in the signaling via toll-like receptor 4-MD-2. Biochem. Biophys. Res. Comm. 268, 172–177.

Amigoni, A., Pettenazzo, A., Stritoni, V., Circelli, M., 2017. Surfactants in acute respiratory distress syndrome in infants and children: past, present and future. Clin. Drug Invest. 37, 729–736.

Andersson, J.M., Grey, C., Larsson, M., Ferreira, T.M., Sparr, E., 2017. Effect of cholesterol on the molecular structure and transitions in a clinical-grade lung surfactant extract. Proc. Natl. Acad. Sci. U. S. A. 114, E3592–E3601.

Autilio, C., Echaide, M., Shankar-Aguilera, S., Bragado, R., Amidani, D., Salomone, F., Pérez-Gil, J., De Luca, D., 2020. Surfactant injury in the early phase of severe meconium aspiration syndrome. Am. J. Resp. Cell Mol. Biol. 63, 327–337.

Backhaus, S., Zakrzewicz, A., Richter, K., Damm, J., Wilker, S., Fuchs-Moll, G., Kullmar, M., Hecker, A., Manzini, I., Ruppert, C., McIntosh, J.M., Padberg, W., Grau, V., 2017. Surfactant inhibits ATP-induced release of interleukin-1beta via nicotinic acetylcholine receptors. J. Lipid Res. 58, 1055–1066.

Bem, R.A., van der Loos, C.M., van Woensel, J.B., Bos, A.P., 2010. Cleaved caspase-3 in lung epithelium of children who died with acute respiratory distress syndrome. Pediatr. Crit. Care Med. 11, 556–560.

Beppu, O.S., Clements, J.A., Goerke, J., 1983. Phosphatidylglycerol-deficient lung surfactant has normal properties. J. Appl. Physiol. Respir. Environ. Exerc. Physiol. 55, 496–502.

Bligh, E.G., Dyer, W.J., 1959. A rapid method of total lipid extraction and purification. Can. J. Biochem. Physiol. 37, 911–917.

Borthwick, L.A., 2016. The IL-1 cytokine family and its role in inflammation and fibrosis in the lung. Sem. Immunopathol. 38, 517–534.

Curstedt, T., Calkovska, A., Johansson, J., 2013. New generation synthetic surfactants. Neonatology 103, 327–330.

de Hoon, M.J., Imoto, S., Nolan, J., Miyano, S., 2004. Open source clustering software. Bioinformatics 20, 1453–1454.

De Luca, D., Lopez-Rodriguez, E., Minucci, A., Vendittelli, F., Gentile, L., Stival, E., Conti, G., Piastra, M., Antonelli, M., Echaide, M., Perez-Gil, J., Capoluongo, E.D., 2013. Clinical and biological role of secretory phospholipase A2 in acute respiratory distress syndrome infants. Crit Care 17, R163.

De Luca, D., van Kaam, A.H., Tingay, D.G., Courtney, S.E., Danhaive, O., Carnielli, V.P., Zimmermann, L.J., Kneyber, M.C.J., Tissieres, P., Brierley, J., Conti, G., Pillow, J.J., Rimensberger, P.C., 2017. The Montreux definition of neonatal ARDS: biological and clinical background behind the description of a new entity. Lancet Respir. Med. 5, 657–666.

Dolinay, T., Kim, Y.S., Howrylak, J., Hunninghake, G.M., An, C.H., Fredenburgh, L., Massaro, A.F., Rogers, A., Gazourian, L., Nakahira, K., Haspel, J.A., Landazury, R., Eppanapally, S., Christie, J.D., Meyer, N.J., Ware, L.B., Christiani, D.C., Ryter, S.W., Baron, R.M., Choi, A.M., 2012. Inflammasome-regulated cytokines are critical mediators of acute lung injury. Am. J. Respir. Crit. Care Med. 185, 1225–1234.

Faix, R.G., Viscardi, R.M., DiPietro, M.A., Nicks, J.J., 1989. Adult respiratory distress syndrome in full-term newborns. Pediatrics 83, 971–976.

Garcia-Verdugo, I., Sanchez-Barbero, F., Soldau, K., Tobias, P.S., Casals, C., 2005. Interaction of SP-A (surfactant protein A) with bacterial rough lipopolysaccharide (*Re*-LPS), and effects of SP-A on the binding of *Re*-LPS to CD14 and LPS-binding protein. Biochem. J. 391, 115–124.

Graessler, J., Schwudke, D., Schwarz, P.E., Herzog, R., Shevchenko, A., Bornstein, S.R., 2009. Top-down lipidomics reveals ether lipid deficiency in blood plasma of hypertensive patients. PLoS ONE 4, e6261.

Grailer, J.J., Canning, B.A., Kalbitz, M., Haggadone, M.D., Dhond, R.M., Andjelkovic, A. V., Zetoune, F.S., Ward, P.A., 2014. Critical role for the NLRP3 inflammasome during acute lung injury. J. Immunol. 192, 5974–5983.

Hallman, M., Gluck, L., 1976. Phosphatidylglycerol in lung surfactant. III. Possible modifier of surfactant function. J. Lipid Res. 17, 257–262.

He, Y., Hara, H., Nunez, G., 2016. Mechanism and regulation of NLRP3 inflammasome activation. Trends Biochem. Sci. 41, 1012–1021.

Herzog, R., Schwudke, D., Schuhmann, K., Sampaio, J.L., Bornstein, S.R., Schroeder, M., Shevchenko, A., 2011. A novel informatics concept for high-throughput shotgun lipidomics based on the molecular fragmentation query language. Genome Biol. 12, R8.

Kandasamy, P., Zarini, S., Chan, E.D., Leslie, C.C., Murphy, R.C., Voelker, D.R., 2011. Pulmonary surfactant phosphatidylglycerol inhibits Mycoplasma pneumoniae-stimulated eicosanoid production from human and mouse macrophages. J. Biol. Chem. 286, 7841–7853.

Keese, S.P., Brandenburg, K., Roessle, M., Schromm, A.B., 2014. Pulmonary surfactant protein A-induced changes in the molecular conformation of bacterial deep-rough LPS lead to reduced activity on human macrophages. Innate Immun. 20, 787–798.

Kolliputi, N., Galam, L., Parthasarathy, P.T., Tipparaju, S.M., Lockey, R.F., 2012. NALP-3 inflammasome silencing attenuates ceramide-induced transepithelial permeability. J. Cell Physiol. 227, 3310–3316.

Kuronuma, K., Mitsuzawa, H., Takeda, K., Nishitani, C., Chan, E.D., Kuroki, Y., Nakamura, M., Voelker, D.R., 2009. Anionic pulmonary surfactant phospholipids inhibit inflammatory responses from alveolar macrophages and U937 cells by binding the lipopolysaccharide-interacting proteins CD14 and MD-2. J. Biol. Chem. 284, 25488–25500.

Liebisch, G., Binder, M., Schifferer, R., Langmann, T., Schulz, B., Schmitz, G., 2006. High throughput quantification of cholesterol and cholesteryl ester by electrospray ionization tandem mass spectrometry (ESI-MS/MS). Biochim. Biophys. Acta 1761, 121–128.

Luzzati, V., Husson, F., 1962. The structure of the liquid-crystalline phasis of lipid-water systems. J. Cell Biol. 2, 207–219.

Luzzati, V., Vargas, R., Mariani, P., Gulik, A., Delacroix, H., 1993. Cubic phases of lipid-containing systems. Elements of a theory and biological connotations. J. Mol. Biol. 229, 540–551.

Mair, K.H., Sedlak, C., Kaser, T., Pasternak, A., Levast, B., Gerner, W., Saalmuller, A., Summerfield, A., Gerdts, V., Wilson, H.L., Meurens, F., 2014. The porcine innate immune system: an update. Dev. Comp. Immunol. 45, 321–343.

Marwitz, S., Depner, S., Dvornikov, D., Merkle, R., Szczygiel, M., Muller-Decker, K., Lucarelli, P., Wasch, M., Mairbaurl, H., Rabe, K.F., Kugler, C., Vollmer, E., Reck, M., Scheufele, S., Kroger, M., Ammerpohl, O., Siebert, R., Goldmann, T., Klingmuller, U., 2016. Downregulation of the TGFbeta pseudoreceptor BAMBI in non-small cell lung cancer enhances TGFbeta signaling and invasion. Cancer Res. 76, 3785–3801.

Minutti, C.M., Jackson-Jones, L.H., Garcia-Fojeda, B., Knipper, J.A., Sutherland, T.E., Logan, N., Ringqvist, E., Guillamat-Prats, R., Ferenbach, D.A., Artigas, A., Stamme, C., Chroneos, Z.C., Zaiss, D.M., Casals, C., Allen, J.E., 2017. Local amplifiers of IL-4Ralpha-mediated macrophage activation promote repair in lung and liver. Science 356, 1076–1080.

Moulakakis, C., Adam, S., Seitzer, U., Schromm, A.B., Leitges, M., Stamme, C., 2007. Surfactant protein A activation of atypical protein kinase C zeta in IkappaB-alpha-dependent anti-inflammatory immune regulation. J. Immunol. 179, 4480–4491.

Mueller, M., Brandenburg, K., Dedrick, R., Schromm, A.B., Seydel, U., 2005. Phospholipids inhibit lipopolysaccharide (LPS)-induced cell activation: a role for LPS-binding protein. J. Immunol. 174, 1091–1096.

Murray, P.J., Wynn, T.A., 2011. Protective and pathogenic functions of macrophage subsets. Nat. Rev. Immunol. 11, 723–737.

Numata, M., Chu, H.W., Dakhama, A., Voelker, D.R., 2010. Pulmonary surfactant phosphatidylglycerol inhibits respiratory syncytial virus-induced inflammation and infection. Proc. Natl. Acad. Sci. U. S. A. 107, 320–325.

Numata, M., Kandasamy, P., Nagashima, Y., Posey, J., Hartshorn, K., Woodland, D., Voelker, D.R., 2012a. Phosphatidylglycerol suppresses influenza A virus infection. Am. J. Res. Cell Mol. Biol. 46, 479–487.

Numata, M., Kandasamy, P., Voelker, D.R., 2012b. Anionic pulmonary surfactant lipid regulation of innate immunity. Expert Rev. Respir.Med. 6, 243–246.

Pelizzi, N., Catinella, S., Barboso, S., Zanol, M., 2002. Different electrospray tandem mass spectrometric approaches for rapid characterization of phospholipid classes of Curosurf, a natural pulmonary surfactant. Rapid Commun. Mass Spectrom. 16, 2215–2220.

Perez-Gil, J., 2008. Structure of pulmonary surfactant membranes and films: the role of proteins and lipid-protein interactions. Biochim. Biophys. Acta 1778, 1676–1695.

Pérez-Gil, J., Keough, K.M., 1998. Interfacial properties of surfactant proteins. Biochim. Biophys. Acta 1408, 203–217.

Preuss, S., Omam, F.D., Scheiermann, J., Stadelmann, S., Winoto-Morbach, S., von Bismarck, P., Adam-Klages, S., Knerlich-Lukoschus, F., Lex, D., Wesch, D., Held-Feindt, J., Uhlig, S., Schutze, S., Krause, M.F., 2012a. Topical application of

phosphatidyl-inositol-3,5-bisphosphate for acute lung injury in neonatal swine. J. Cell. Mol. Med. 16, 2813–2826.
Preuss, S., Stadelmann, S., Omam, F.D., Scheiermann, J., Winoto-Morbach, S., von Bismarck, P., Knerlich-Lukoschus, F., Lex, D., Adam-Klages, S., Wesch, D., Held-Feindt, J., Uhlig, S., Schutze, S., Krause, M.F., 2012b. Inositol-trisphosphate reduces alveolar apoptosis and pulmonary edema in neonatal lung injury. Am. J. Resp. Cell Mol. Biol. 47, 158–169.
Ricci, F., Murgia, X., Razzetti, R., Pelizzi, N., Salomone, F., 2017. *In vitro* and *in vivo* comparison between poractant alfa and the new generation synthetic surfactant CHF5633. Pediatr. Res. 81, 369–375.
Saldanha, A.J., 2004. Java Treeview–extensible visualization of microarray data. Bioinformatics 20, 3246–3248.
Schwudke, D., Hannich, J.T., Surendranath, V., Grimard, V., Moehring, T., Burton, L., Kurzchalia, T., Shevchenko, A., 2007. Top-down lipidomic screens by multivariate analysis of high-resolution survey mass spectra. Anal. Chem. 79, 4083–4093.
Sender, V., Lang, L., Stamme, C., 2013. Surfactant protein-A modulates LPS-induced TLR4 localization and signaling via beta-arrestin 2. PLoS ONE 8, e59896.
Spengler, D., Winoto-Morbach, S., Kupsch, S., Vock, C., Blochle, K., Frank, S., Rintz, N., Diekotter, M., Janga, H., Weckmann, M., Fuchs, S., Schromm, A.B., Fehrenbach, H., Schutze, S., Krause, M.F., 2018. Novel therapeutic roles for surfactant-inositols and -phosphatidylglycerols in a neonatal piglet ARDS model: a translational study. Am. J. Physiol. Lung Cell. Mol. Physiol. 314, L32–L53.
Stamme, C., Müller, M., Hamann, L., Gutsmann, T., Seydel, U., 2002. Surfactant protein a inhibits lipopolysaccharide-induced immune cell activation by preventing the interaction of lipopolysaccharide with lipopolysaccharide-binding protein. Am. J. Respir. Cell Mol. Biol. 27, 353–360.
Sweet, D.G., Turner, M.A., Stranak, Z., Plavka, R., Clarke, P., Stenson, B.J., Singer, D., Goelz, R., Fabbri, L., Varoli, G., Piccinno, A., Santoro, D., Speer, C.P., 2017. A first-in-human clinical study of a new SP-B and SP-C enriched synthetic surfactant (CHF5633) in preterm babies with respiratory distress syndrome. Arch. Dis. Child. Fetal Neonatal Ed. 102, F497–F503.
Todd, D.A., Marsh, M.J., George, A., Henderson, N.G., Barr, H., Sebastian, S., Clark, G.T., Koster, G., Clark, H.W., Postle, A.D., 2010. Surfactant phospholipids, surfactant proteins, and inflammatory markers during acute lung injury in children. Pediatr. Crit. Care Med. 11, 82–91.
Wright, J.R., 2005. Immunoregulatory functions of surfactant proteins. Nat. Rev. Immunol. 5, 58–68.
Xu, L., Yang, Y., Zuo, Y.Y., 2020. Atomic force microscopy imaging of adsorbed pulmonary surfactant films. Biophys. J. 119, 756–766.